

We are IntechOpen, the world's leading publisher of Open Access books Built by scientists, for scientists

6,900

Open access books available

186,000

International authors and editors

200M

Downloads

Our authors are among the

154

Countries delivered to

TOP 1%

most cited scientists

12.2%

Contributors from top 500 universities



WEB OF SCIENCE™

Selection of our books indexed in the Book Citation Index
in Web of Science™ Core Collection (BKCI)

Interested in publishing with us?
Contact book.department@intechopen.com

Numbers displayed above are based on latest data collected.
For more information visit www.intechopen.com



A Kinematical and Dynamical Analysis of a Quadruped Robot

Alain Segundo Potts and José Jaime da Cruz
*University of São Paulo
Brazil*

1. Introduction

In general, legged locomotion requires higher degrees of freedom and therefore greater mechanical complexity than wheeled locomotion. Wheeled robots are simple in general, and more efficient than legged locomotion on flat surfaces. Yet as the surface turns softer, wheeled locomotion becomes inefficient due to rolling friction. Furthermore, in some cases, wheeled robots are unable to overcome small obstacles. On the other hand, legged robots are more easily adaptable to different kinds of terrains due to the fact that only a set of point contacts is required; thus, the quality of the ground between those points does not matter as long as the robot can maintain appropriate ground clearance.

Legged robots appear as the sole means of providing locomotion in highly unstructured environments. However, they cannot traverse every type of uneven terrain because they are of limited dimensions. Hence, if there are terrain irregularities such as a crevasse wider than the maximum horizontal leg reach or a cliff of depth greater than the maximum vertical leg reach, then the machine is prevented from making any progress. This limitation, however, can be overcome by providing the machine with the capability of attaching its feet to the terrain. Moreover, machine functionality is limited not only by the topography of the terrain, but also by the terrain constitution. Whereas hard rock poses no serious problem to legged robots, muddy terrain can hamper its operation to the point of jamming the machine. Still, under such adverse conditions, legged robots offer a better maneuverability than other vehicles (Angeles, 2007; Siegwart & Nourbakhsh, 2004).

The main disadvantages of legged locomotion include power and mechanical complexity. The leg, which may include several degrees of freedom, must be capable of sustaining part of the robot's total weight and, in many robots, must be capable of lifting and lowering the robot. Additionally, high maneuverability will only be achieved if the legs have a sufficient number of degrees of freedom to impart forces in a number of different directions.

In the last few years, this feature has given rise to a number of research activities on the subject. Despite all these efforts, the performance of legged robots is still far from what could be expected from them. This is true particularly because the robots performance depends on several factors, including the mechanical design, which sometimes may not be changed by the control designer (Estremera & Waldron, 2008).

Legged robots present some problems that are not usual in wheeled robots. For example, problems such as trajectory planning and stability analysis need a good kinematics and dynamics model of the system.

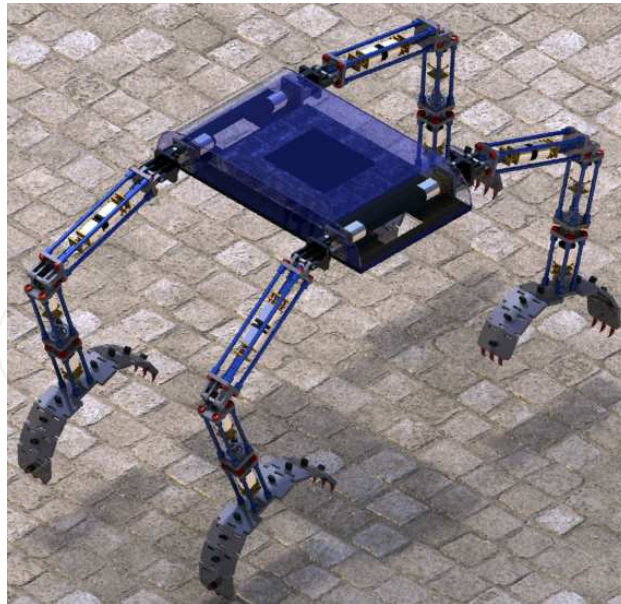


Fig. 1. Kamambaré I robot

Herein will be presented a kinematical and dynamical analysis of a quadruped robot named Kamambaré I (Bernardi & Da Cruz, 2007).

Like all the mobile robots with legs the topology of Kamambaré is time variant. Due to his own gait, we have two different problems to solve. First when there is at least one closed kinematic chain between the support surface and the platform, the robot's behavior will be similar to a parallel robot. On the other hand, when a leg of the robot is in the air looking for a new point of grasping, the model that best describes it is an open kinematic chain model, similar to the models of a serial industrial manipulator. Through this work we will refer to these two topological models as the platform for the parallel case of modeling and model of the leg for the second case reviewed like in (Potts & Da Cruz, 2010).

The analysis above, is important for bringing the platform or the gripper to some desired position in the space, but in our case it is not sufficient. To move the platform or the gripper along some desired path with a prescribed speed, the motion of the joints must be carefully coordinated. There are two types of velocity coordination problems, direct and inverse. In the first case, the velocity of the joints is given and the objective is to find the velocity of the end effector (platform or leg); in the other case, the velocity of the end effector is given and the input joint rates required to produce the desired velocity are to be found.

2. Kinematics model

Kamambaré I is a symmetrical quadruped robot. It was developed for climbing vertical objects such as trees, power poles, bridges, etc. Each of its legs with four revolution joints. See Fig. 1. At the end of each leg, there is a gripper. All joints are powered by DC motors.

The basic gait of the robot simulates the walking trot of a quadruped mammal. In this type of gait, the diagonal legs move in tandem. While a pair of legs is fixed to the supporting surface and pushes the robot forward the other pair is on the air, seeking a new foothold, see Figure 2. According to that description, there are two basic stages for the legs, which will be named: "leg on the air" to represent the leg seeking for the new foothold, and "pushing stage" when the leg is fixed and pushing the body to a given direction.

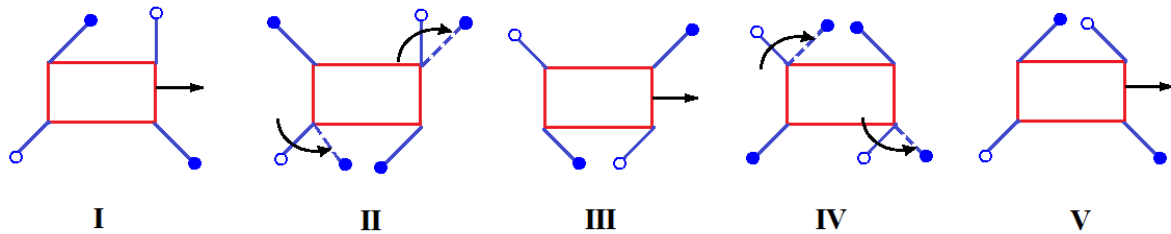


Fig. 2. Gait graphs for the trot of the Kamambaré robot. Leg on the air \circ , leg attached to the surface \bullet .

For a robot to move to a specific position, the location of the center of its body relative to the base should be established first. This is called by some authors *position analysis problem* (Tsai, 1999). There are two types of position analysis problems: direct kinematics and inverse kinematics problems. In the first one, the joint variables are given and the problem is to find the location of the body of the robot; for the inverse kinematics, the location of the body is given and the problem is to find the joint variables that correspond to it (Kolter et al., 2008). Two approaches will be taken herein for the complete modeling of the robot in accordance with its topology. Firstly, for the robot in the pushing stage the model will be like a parallel robot with a closed chain between the two legs that are supporting the platform. Then when the leg is “on the air” the model is of a serial manipulator attached at one of the corners of the platform.

2.1 Direct kinematics problem of the platform

In this section, the direct kinematics problem of the platform will be solved. The system is modeled as a parallel robot and the legs are stuck between the supporting surface and the platform. The analysis is performed using the Denavit-Hartenberg (D-H) parametrization, starting at the surface and advancing towards the platform.

i	α_{i-1}	a_{i-1}	d_i	θ_i
4	0	0	L_4	θ_{4l}
3	$\frac{\pi}{2}$	0	0	θ_{3l}
2	0	L_3	0	θ_{2l}
1	$-\frac{\pi}{2}$	L_2	0	θ_{1l}
	0	L_1	0	0

Table 1. Denavit-Hartenberg parameters for leg l in the pushing stage

Table 1 shows the D-H parameters for the “pushing stage”. Frames $\{B_l\}$, $\{C_l\}$, $\{D_l\}$ and $\{E_l\}$ are attached to links 4, 3, 2 and 1, respectively, as shown by Figure 3. Frame $\{O\}$ is attached at a point of the climbing surface, $\{A_l\}$ is attached to the gripping point and $\{P\}$ is attached to the robotic platform. The lengths of the links are L_5 , L_4 , L_3 , L_2 and L_1 , respectively, starting at the point ${}^O A_l$, origin of the frame $\{A_l\}$. Index l , ($l = 1, \dots, 4$) is used to indicate the leg of the robot, while index i , ($i = 1, \dots, 4$) is used to indicate the i -th joint of the l -th leg. In this paper, vector ${}^O A_l \vec{B}_l$ relative to frame $\{O\}$ is assumed to be orthogonal to the climbing surface, (Bernardi et al., 2009).

Denoting by ${}^{Y_l} T_{X_l}$ the homogeneous transformation from the coordinate systems $\{X_l\}$ to coordinate system $\{Y_l\}$ of the l -th leg, ${}^O T_P$ can be expressed as:

$${}^O T_P = {}^O T_{A_l} \cdot {}^{A_l} T_{B_l} \cdot {}^{B_l} T_{C_l} \cdot {}^{C_l} T_{D_l} \cdot {}^{D_l} T_{E_l} \cdot {}^{E_l} T_P \tag{1}$$

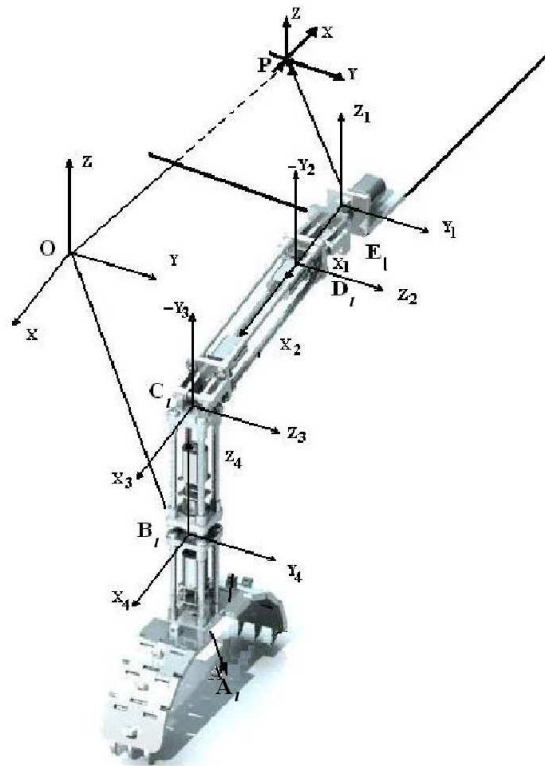


Fig. 3. Scheme of l -th leg.

Recalling that the structure of ${}^O T_{A_l}$, ${}^{A_l} T_{B_l}$ and ${}^{B_l} T_P$ are:

$${}^O T_{A_l} = \begin{bmatrix} {}^O R_{A_l} & | & {}^O \vec{O}A_l \\ \hline \mathbf{0} & | & 1 \end{bmatrix}, \quad (2)$$

$${}^{A_l} T_{B_l} = \begin{bmatrix} {}^{A_l} R_{B_l} & | & {}^{A_l} \vec{A_l}B_l \\ \hline \mathbf{0} & | & 1 \end{bmatrix} \quad (3)$$

and

$${}^{B_l} T_P = \begin{bmatrix} {}^{B_l} R_P & | & {}^{B_l} \vec{B_l}P \\ \hline \mathbf{0} & | & 1 \end{bmatrix}, \quad (4)$$

Assume that matrixes ${}^O R_{A_l}$ and ${}^{A_l} R_{B_l}$ are equal to identity matrix I and due to a sequence of straightforward computations the rotation matrix ${}^{B_l} R_P$ is equal to:

$${}^{B_l} R_P = \begin{bmatrix} c\theta_{4_l} c\theta_{2_l 3_l} c\theta_{1_l} + s\theta_{4_l} s\theta_{1_l} & -c\theta_{4_l} c\theta_{2_l 3_l} s\theta_{1_l} + s\theta_{4_l} c\theta_{1_l} & c\theta_{4_l} s\theta_{2_l 3_l} \\ s\theta_{4_l} c\theta_{2_l 3_l} c\theta_{1_l} - c\theta_{4_l} s\theta_{1_l} & -s\theta_{4_l} c\theta_{2_l 3_l} s\theta_{1_l} - c\theta_{4_l} c\theta_{1_l} & s\theta_{4_l} s\theta_{2_l 3_l} \\ s\theta_{2_l 3_l} c\theta_{1_l} & -s\theta_{2_l 3_l} s\theta_{1_l} & -c\theta_{2_l 3_l} \end{bmatrix} \quad (5)$$

and to the position of the origin of system $\{P\}$ with respect to $\{B\}$

$${}^O \vec{B_l}P = \begin{bmatrix} (c\theta_{4_l} c\theta_{2_l 3_l} c\theta_{1_l} + s\theta_{4_l} s\theta_{1_l})L_1 + c\theta_{4_l} (c\theta_{2_l 3_l} L_2 + c\theta_{3_l} L_3) \\ (s\theta_{4_l} c\theta_{2_l 3_l} c\theta_{1_l} - c\theta_{4_l} s\theta_{1_l})L_1 + s\theta_{4_l} (c\theta_{2_l 3_l} L_2 + c\theta_{3_l} L_3) \\ s\theta_{2_l 3_l} c\theta_{1_l} L_1 + s\theta_{2_l 3_l} L_2 + s\theta_{3_l} L_3 + L_4 \end{bmatrix} \quad (6)$$

for $l = 1, 2, 3, 4,$.

Then, using 6, the direct kinematics problem of the platform can be solved by the vector equation:

$${}^O\vec{OP} = {}^O\vec{OA}_l + {}^O\vec{A}_l\vec{B}_l + {}^O\vec{B}_l\vec{P} \tag{7}$$

for a know coordinates of points ${}^O A_l$ and ${}^O B_l$ relatives to frame $\{O\}$.

2.2 Direct kinematics problem of the leg

Since any homogeneous transformation matrix ${}^{Y_l}T_{X_l}$ is non-singular it is possible to use that expression to solve the direct kinematics problem for the leg on the air:

$${}^{E_l}T_{A_l} = \left[\begin{array}{c|c} {}^{E_l}R_{A_l} & {}^{E_l}E_l\vec{A}_l \\ \hline \mathbf{0} & 1 \end{array} \right] \tag{8}$$

where:

$${}^{E_l}R_{A_l} = \left[\begin{array}{ccc} c\theta_{4_l}c\theta_{2_l3_l}c\theta_{1_l} + s\theta_{4_l}s\theta_{1_l} & s\theta_{4_l}c\theta_{2_l3_l}c\theta_{1_l} - c\theta_{4_l}s\theta_{1_l} & c\theta_{1_l}s\theta_{2_l3_l} \\ -c\theta_{4_l}c\theta_{2_l3_l}s\theta_{1_l} + s\theta_{4_l}c\theta_{1_l} & -s\theta_{4_l}c\theta_{2_l3_l}s\theta_{1_l} - c\theta_{4_l}c\theta_{1_l} & -s\theta_{1_l}s\theta_{2_l3_l} \\ s\theta_{2_l3_l}c\theta_{4_l} & s\theta_{2_l3_l}s\theta_{4_l} & -c\theta_{2_l3_l} \end{array} \right] \tag{9}$$

and the position of the gripper relative to frame $\{E_l\}$ is given by:

$${}^{E_l}E_l\vec{A}_l = \left[\begin{array}{c} (c\theta_{2_l3_l}\bar{L}_4 + c\theta_{2_l}L_3 + L_2)c\theta_{1_l} \\ (c\theta_{2_l3_l}\bar{L}_4 + c\theta_{2_l}L_3 + L_2)s\theta_{1_l} \\ s\theta_{2_l3_l}\bar{L}_4 - s\theta_{2_l}L_3 \end{array} \right] \tag{10}$$

where $\bar{L}_4 = L_4 + L_5$

The use of 4 or 8 depends on which part of the gait is active. In other words, if the leg l of the robot is in the air, the transformations between joint frames occur based on the frame $\{E_l\}$. On the other hand, if the leg is clung to the surface, the reference coordinate system is $\{O\}$.

2.3 Inverse kinematics problem for the platform

Since each leg has only four degrees of freedom, the position and orientation of the platform must be specified in accordance with the constraints imposed by the joints.

Using equations 7 and 6, it is possible to solve the inverse kinematics problem. If both, clinging point ${}^O A_l$ and the position and orientation of the platform $[{}^O P_x, {}^O P_y, {}^O P_z, \psi_P]$ are given as well as the geometrical and mathematical constraints are respected, from equation 6 we have:

$$c\theta_{4_l} = \frac{y_{PAB_l}s\psi_P L_1 \pm x_{PAB_l}\sqrt{x_{PAB_l}^2 + y_{PAB_l}^2 - s\psi_P^2 L_1^2}}{x_{PAB_l}^2 + y_{PAB_l}^2} \tag{11}$$

where: $x_{PAB_l} = {}^O P_x - {}^O A_{x_l} - {}^O B_{x_l}$ and $y_{PAB_l} = {}^O P_y - {}^O A_{y_l} - {}^O B_{y_l}$.

Equation 11 is subject to:

$$x_{PAB_l}^2 + y_{PAB_l}^2 \neq 0, \tag{12}$$

$$x_{PAB_l}^2 + y_{PAB_l}^2 \geq s\psi_P^2 L_1^2 \tag{13}$$

and

$$\left| \frac{y_{PAB_l} s\psi_P L_1 \pm x_{PAB_l} \sqrt{x_{PAB_l}^2 + y_{PAB_l}^2 - s\psi_P^2 L_1^2}}{x_{PAB_l}^2 + y_{PAB_l}^2} \right| \leq 1. \quad (14)$$

Whit respect to θ_{2_l} we have:

$$c\theta_{2_l} = \frac{x_{PAB_l}^2 + y_{PAB_l}^2 + z_{PAB_l}^2 - L_3^2 - \bar{L}_2^2 - s\psi_P^2 L_1^2}{2L_3 \bar{L}_2} \quad (15)$$

where $\bar{L}_2 = c\psi_P L_1 + L_2$ and $z_{PAB_l} = {}^{O_P}z - {}^{O_{A_{z_l}}}z - {}^{O_{B_{z_l}}}z - L_4$.

As $|c\theta_{2_l}| \leq 1$, equation 15 is subject to:

$$x_{PAB_l}^2 + y_{PAB_l}^2 + z_{PAB_l}^2 \leq (L_3 + L_2)^2 + 2L_1 c\psi_P (L_3 + L_2) + L_1^2 \quad (16)$$

and

$$x_{PAB_l}^2 + y_{PAB_l}^2 + z_{PAB_l}^2 \geq (L_3 - L_2)^2 - 2L_1 c\psi_P (L_3 - L_2) + L_1^2 \quad (17)$$

finally

$$s\theta_{3_l} = \frac{(c\theta_{2_l} \bar{L}_2 + L_3) z_{PAB_l} \pm s\theta_{2_l} \bar{L}_2 \sqrt{L_3^2 + 2c\theta_{2_l} L_3 \bar{L}_2 + \bar{L}_2^2 - z_{PAB_l}^2}}{L_3^2 + 2c\theta_{2_l} L_3 \bar{L}_2 + \bar{L}_2^2} \quad (18)$$

subject to:

$$L_3^2 + 2c\theta_{2_l} L_3 \bar{L}_2 + \bar{L}_2^2 - z_{PAB_l}^2 \geq 0, \quad (19)$$

$$L_3^2 + 2c\theta_{2_l} L_3 \bar{L}_2 + \bar{L}_2^2 \neq 0, \quad (20)$$

and

$$\left| \frac{(c\theta_{2_l} \bar{L}_2 + L_3) z_{PAB_l} \pm s\theta_{2_l} \bar{L}_2 \sqrt{L_3^2 + 2c\theta_{2_l} L_3 \bar{L}_2 + \bar{L}_2^2 - z_{PAB_l}^2}}{L_3^2 + 2c\theta_{2_l} L_3 \bar{L}_2 + \bar{L}_2^2} \right| \leq 1 \quad (21)$$

the last constraints are verified when relation 13 and $x_{PAB_l}^2 + y_{PAB_l}^2 + z_{PAB_l}^2 - s\psi_P^2 L_1^2 \neq 0$ are satisfied for $l = 1, 2, 3, 4$. In addition, from 19 and 20: $z_{PAB_l} \neq 0$.

Hence, the inverse kinematics problem is solved. Now the orientation of the body has to be defined. A usual way of defining it is through the Euler angles. Denoting by ϕ_P , θ_P and ψ_P the Euler angles associated to Z-Y-Z convention, the rotation matrix with respect to system $\{O\}$, ${}^O\bar{R}_P$, is given by:

$${}^O\bar{R}_P = \begin{bmatrix} c\phi_P c\theta_P c\psi_P - s\phi_P s\psi_P & -c\phi_P c\theta_P s\psi_P - s\phi_P c\psi_P & c\phi_P s\theta_P \\ s\phi_P c\theta_P c\psi_P + c\phi_P s\psi_P & -s\phi_P c\theta_P s\psi_P + c\phi_P s\psi_P & s\phi_P s\theta_P \\ -s\theta_P c\psi_P & s\theta_P s\psi_P & c\theta_P \end{bmatrix} \quad (22)$$

Equaling 5 and 22 it follow that:

$$c\theta_P = -c\theta_{2,3_l}, \quad (23)$$

$$t\psi_P = t\theta_{1_l}, \quad (24)$$

and

$$t\phi_P = t\theta_{4_l}, \quad (25)$$

where $\theta \neq 0, \pi$ for $l = 1, 2, 3, 4$.

As said in the last section, angles θ_{2_l} , θ_{3_l} and θ_{4_l} are not independent. Hence, $\theta_P = f(P_x, P_y, P_z, \theta_{1_l})$ and $\phi_P = f(P_x, P_y, P_z, \theta_{1_l})$ for a given point ${}^O A_l$.

2.4 Inverse kinematics problem for the leg

In this section, the inverse kinematics problem for the leg on the air will be solved. The starting point for the solution of the inverse kinematic problem of the gripper is equation 10. For points ${}^{E_l} E_l$ and ${}^{E_l} A_l$ given, the solution is:

$$t\theta_{1_l} = \frac{y_{AE_l}}{x_{AE_l}} \quad (26)$$

where:

$$x_{AE_l} = {}^{E_l} A_{x_l} - {}^{E_l} E_{x_l}, y_{AE_l} = {}^{E_l} A_{y_l} - {}^{E_l} E_{y_l}, c\theta_{1_l} \neq 0$$

and

$$x_{AE_l} \neq 0$$

After finding θ_{1_l} , the next step is to compute θ_{3_l} :

$$c\theta_{3_l} = \frac{x_{AE_l}^2 + y_{AE_l}^2 \pm 2L_2 \sqrt{x_{AE_l}^2 + y_{AE_l}^2} + z_{AE_l}^2 + L_2^2 - \bar{L}_4^2 - L_3^2}{2\bar{L}_4 L_3} \quad (27)$$

where: $x_{AE_l}^2 + y_{AE_l}^2 \neq 0$ and

$$(\bar{L}_4 + L_3)^2 \leq \left(\sqrt{x_{AE_l}^2 + y_{AE_l}^2} - L_2 \right)^2 + z_{AE_l}^2 \leq (\bar{L}_4 - L_3)^2 \quad (28)$$

Finally:

$$s\theta_{2_l} = \frac{z_{AE_l}(c\theta_{3_l}L_4 + L_3) \pm s\theta_{3_l}L_4 \sqrt{L_4^2 + 2c\theta_{3_l}L_4L_3 + L_3^2 - z_{AE_l}^2}}{\bar{L}_4^2 + 2c\theta_{3_l}L_3L_4 + L_3^2} \quad (29)$$

where:

$$L_4^2 + 2c\theta_{3_l}L_4L_3 + L_3^2 - z_{AE_l}^2 \geq 0, \quad (30)$$

$$L_4^2 + 2c\theta_{3_l}L_4L_3 + L_3^2 \neq 0 \quad (31)$$

and

$$\left| \frac{z_{AE_l}(c\theta_{3_l}L_4 + L_3) \pm s\theta_{3_l}L_4 \sqrt{L_4^2 + 2c\theta_{3_l}L_4L_3 + L_3^2 - z_{AE_l}^2}}{\bar{L}_4^2 + 2c\theta_{3_l}L_3L_4 + L_3^2} \right| \leq 1 \quad (32)$$

Inequations 30, 31 and 32 are satisfied for:

$$c\theta_{3_l} \neq -\frac{L_4^2 + L_3^2}{2L_4L_3}, \quad (33)$$

and

$$x_{AE_l}^2 + y_{AE_l}^2 \geq L_2^2 \quad (34)$$

Besides from 30 and 31 we have the condition $z_{AE_l} \neq 0$. Equations 26, 27 and 29 give multiples solutions for the system. The orientation of gripper is represent by φ_l and its value coincides directly with the value of θ_{4_l}

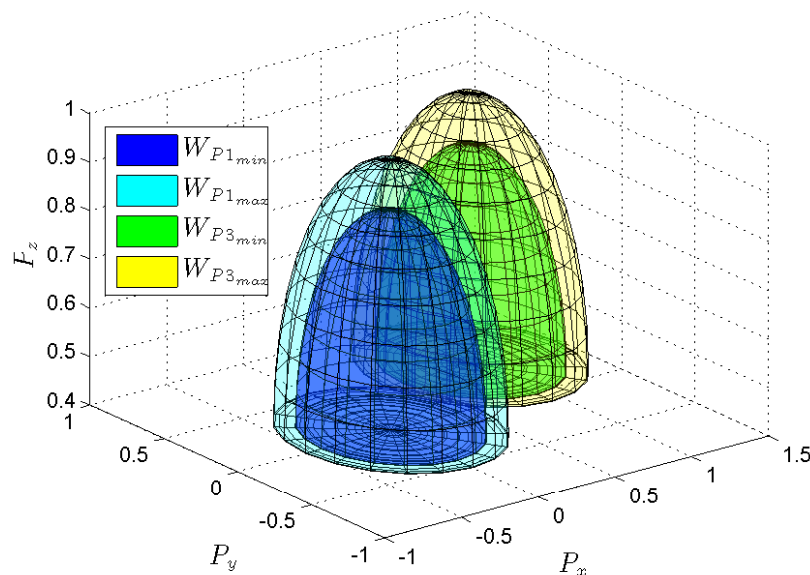


Fig. 4. Workspaces of the center of platform associated to legs 1 and 3.
 ($\mathcal{W}_{P_1} = \mathcal{W}_{P_{1max}} - \mathcal{W}_{P_{1min}}$ and $\mathcal{W}_{P_3} = \mathcal{W}_{P_{3max}} - \mathcal{W}_{P_{3min}}$)

2.5 Workspace

The workspace is formed by the set of points of the reachable workspace where the robot can generate velocities that span the complete tangent space at that point.

The relationships between joint space and Cartesian space coordinates are generally multiple-valued: the same position can be reached in different ways, each with a different set of joint coordinates. Hence, the reachable workspace of the robot is formed by the configurations, in which the kinematic relationships are locally one-to-one (Pieper, 1968).

2.6 Workspace of the platform

The workspace of the platform is formed by the set of points $P = (P_x, P_y, P_z)$ that satisfy equation 7 subject to constraints imposed by 13 and 17.

In a graphic form was defined by \mathcal{W}_{P_l} , the workspace of the center of platform relative to leg l , and if there is more than one leg support the platform the final workspace will be the intersection of all the \mathcal{W}_{P_l} of the legs clung to the surface. In a general case:

$$\mathcal{W}_P = \mathcal{W}_{P_1} \cap \mathcal{W}_{P_2} \cap \dots \mathcal{W}_{P_4} \quad (35)$$

Figure 4 show the workspace formed by the intersection of set \mathcal{W}_{P_1} and \mathcal{W}_{P_3} , and sets $\mathcal{W}_{P_{lmin}}$ and $\mathcal{W}_{P_{lmax}}$ represents the minimum and maximum values of the workspace of each legs. The lengths of the limbs are showed in table 2.

2.7 Workspace of the leg

The workspace of leg \mathcal{W}_{G_l} , when it is in the air, corresponds to its reachable Cartesian space. In this case, \mathcal{W}_{G_l} is formed by the admissible solutions of equations 28. The geometrical form of this workspace is shown in figure 5.

Table 2. Dimensions of the limbs

Limbs	Length(m)	Weight(kg)	Moment of Inertia($N - m^2$)
L_5	0.2	0.25	$1.25 \cdot 10^{-5}$
L_4	0.2	0.2	$17.6 \cdot 10^{-5}$
L_3	0.3	0.25	$130.83 \cdot 10^{-5}$
L_2	0.1	0.06	$1.625 \cdot 10^{-5}$
Platform: (L_1)	0.3	5.25	$2932.45 \cdot 10^{-5}$

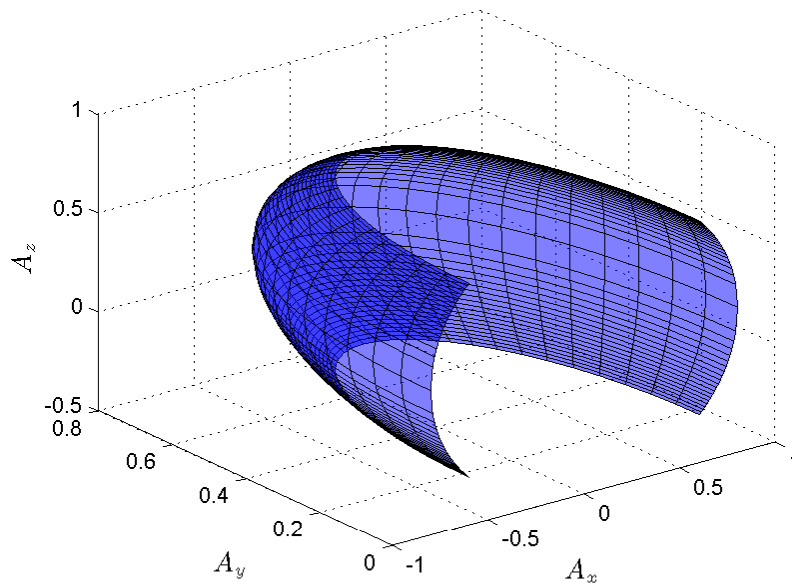


Fig. 5. Workspace for the gripper.

3. Singularity analysis

In previous sections, the problems of direct and inverse kinematics were discussed, both for the platform and for the leg. Such analysis is important for bringing the platform or the gripper to some desired position in the space, but in our case it is not sufficient. The motion of the joints must be carefully coordinated to move the platform or the gripper along some desired path with a prescribed speed. There are two types of velocity coordination problems namely, direct and inverse. In the first case, the velocity of the joints is given and the objective is to find the velocity state of the end effector (platform or leg); in the later case, the velocity state of the end effector is given and the input joint rates required to produce the desired velocity are to be found. (Tsai, 1999)

Thus, the matrix that transforms the joint rates in the actuator space into the velocity state in the end effector space is called Jacobian matrix.

3.1 Singularity analysis for the platform

Due to the characteristics of the gait chosen for the robot, there will always be a closed-chain kinematics formed by the legs clung to the climbing surface. The closed-chain is also characterized by a set of inputs (denoted here by a vector \mathbf{q}), which correspond to the powered joints, and by a set of output coordinates (denoted here by a vector \mathbf{x}). These input and output vectors depend on the nature and purpose of the kinematics chain (Goselin & Angeles, 1990).

The orientation of the platform relative to system $\{O\}$ is given by matrix ${}^O R_P$. Then the platform angular velocity with respect to $\{O\}$, is:

$$\begin{bmatrix} {}^O \omega_{p_x} \\ {}^O \omega_{p_y} \\ {}^O \omega_{p_z} \end{bmatrix} = \begin{bmatrix} 0 & -s\phi_P & s\theta_P c\phi_P \\ 0 & c\phi_P & s\theta_P s\phi_P \\ 1 & 0 & c\theta_P \end{bmatrix} \begin{bmatrix} \dot{\phi}_P \\ \dot{\theta}_P \\ \dot{\psi}_P \end{bmatrix} \quad (36)$$

The linear velocity of point E_l is given by

$${}^O \vec{v}_{E_l} = {}^O \vec{v}_P + {}^O \vec{\omega}_p \times ({}^O R_P \cdot {}^O \vec{P}E_l) \quad (37)$$

where ${}^O \vec{v}_{E_l}$ and ${}^O \vec{v}_P$ are respectively the linear velocities of points E_l and P , with respect to $\{O\}$.

The left-hand side of 37 can be rewritten as:

$${}^O \vec{v}_{E_l} = J_{q_l} \begin{bmatrix} \dot{\theta}_{4_l} \\ \dot{\theta}_{3_l} \\ \dot{\theta}_{2_l} \end{bmatrix} \quad (38)$$

where:

$$J_{q_l} = \begin{bmatrix} -s\theta_{4_l}(c\theta_{3_l}L_2 + c\theta_{3_l}L_3) & -c\theta_{4_l}(s\theta_{3_l}L_2 + s\theta_{3_l}L_3) & -c\theta_{4_l}L_2s\theta_{3_l} \\ c\theta_{4_l}(c\theta_{3_l}L_2 + c\theta_{3_l}L_3) & -s\theta_{4_l}(s\theta_{3_l}L_2 + s\theta_{3_l}L_3) & -s\theta_{4_l}L_2s\theta_{3_l} \\ 0 & c\theta_{3_l}L_2 + c\theta_{3_l}L_3 & c\theta_{3_l}L_2 \end{bmatrix} \quad (39)$$

On the right-hand side of 37, the product ${}^O \vec{\omega}_p \times ({}^O R_P \cdot \vec{P}E_l)$ can be rewritten as:

$${}^O \vec{\omega}_p \times ({}^O R_P \cdot \vec{P}E_l) = \Omega_{F_l} \begin{bmatrix} {}^O \omega_{p_x} \\ {}^O \omega_{p_y} \\ {}^O \omega_{p_z} \end{bmatrix} \quad (40)$$

where:

$$\Omega_{F_l} = \begin{bmatrix} 0 & Y_{z_l} & -Y_{y_l} \\ -Y_{z_l} & 0 & Y_{x_l} \\ Y_{y_l} & -Y_{x_l} & 0 \end{bmatrix} \quad (41)$$

and $\vec{Y}_l = {}^O R_P \cdot \vec{P}E_l$

Substituting 36 and 40 into 37 gives:

$${}^O \vec{v}_{E_l} = J_{x_1} J_{x_2} \begin{bmatrix} {}^O v_{P_x} \\ {}^O v_{P_y} \\ {}^O v_{P_z} \\ \dot{\phi} \\ \dot{\theta} \\ \dot{\psi} \end{bmatrix} \quad (42)$$

where:

$$J_{x_1} = [I_{3 \times 3} \quad \Omega_{F_l}] \quad (43)$$

and

$$J_{x_2} = \begin{bmatrix} I_{3 \times 3} & 0_{3 \times 3} \\ 0_{3 \times 3} & \begin{bmatrix} 0 & -s\phi_P & s\theta_P c\phi_P \\ 0 & c\phi_P & s\theta_P s\phi_P \\ 1 & 0 & c\theta_P \end{bmatrix} \end{bmatrix} \quad (44)$$

Finally, for the four legs:

$$J_q \vec{q} = J_x \vec{x}_p \quad (45)$$

where:

$$J_x = J_{x_{p1}} J_{x_2}, \quad (46)$$

$$J_q = \text{diag}(J_{q_1}, \dots, J_{q_4}), \quad (47)$$

$$J_{x_{p1}} = \begin{bmatrix} I_{3 \times 3} & \Omega_{F_1} \\ \vdots & \vdots \\ I_{3 \times 3} & \Omega_{F_4} \end{bmatrix}, \quad (48)$$

$\vec{q} = [\theta_{4_1}, \theta_{3_1}, \theta_{2_1}, \dots, \theta_{4_4}, \theta_{3_4}, \theta_{2_4}]^T$ and $\vec{x}_p = [x_p, y_p, z_p, \phi_p, \theta_p, \psi_p]^T$.

The elements of \vec{q} correspond to the set of active joints. This set may vary with the robot gait, with the number of legs clung to the climbing surface and with the eventual use of an optimal control policy.

Vector \vec{x}_p contains the position and the Euler angles that define the orientation of the platform. When the lengths of the input and output vectors are not the same, there are redundancies (Lenarcic & Roth, 2006). These are eliminated when there are only two legs holding the robot: $\vec{q} = [\theta_{4_1}, \theta_{3_1}, \theta_{2_1}, \theta_{4_3}, \theta_{3_3}, \theta_{2_3}]$. Variables $x_p, y_p, z_p, \phi_p, \theta_p$ and ψ_p are not all arbitrary, but must satisfy the constraints imposed on the kinematics equations.

3.1.1 Inverse Kinematics Singularity of the platform:

Inverse kinematics singularity occurs when:

$$\det(J_q) = 0. \quad (49)$$

This kind of singularity consists of the set of points where different branches of the inverse kinematics problem meet, being the inverse kinematics problem understood here as the computation of the values of the input variables from given values of the output variables. Since the dimension of the null space of J_q is nonzero in the presence of a singularity of this kind, we can find nonzero vectors \vec{q} for which \vec{x} will be equal to zero and, therefore, some of the velocity vectors $\dot{\vec{q}}$ cannot be produced at the output (Goselin & Angeles, 1990).

From 47, it follows that

$$\det(J_q) = \det(J_{q_1}) \det(J_{q_2}) \det(J_{q_3}) \det(J_{q_4}) \quad (50)$$

where, from 39,

$$\det(J_{q_l}) = -L_2 L_3 s\theta_{2_l} (c\theta_{2_l} L_2 + c\theta_{3_l} L_3) \quad (51)$$

for $l = 1, \dots, 4$.

The singularities occur when $\theta_{2_l} = 0, \pm\pi, \dots, \pm n\pi, \forall n \in \mathbb{N}$ or when:

$$c\theta_{3_l} = \pm \frac{|s\theta_{2_l}|}{\sqrt{\frac{L_3^2}{L_2^2} + 2\frac{L_3}{L_2} c\theta_{2_l} + 1}} \quad (52)$$

where:

$$c\theta_{2_l} > -\frac{\frac{L_3^2}{L_2^2} + 1}{2\frac{L_3}{L_2}} \quad (53)$$

for $l = 1, \dots, 4$.

According to 52, for a given value of θ_{2_l} , there will be two solutions for θ_{3_l} .

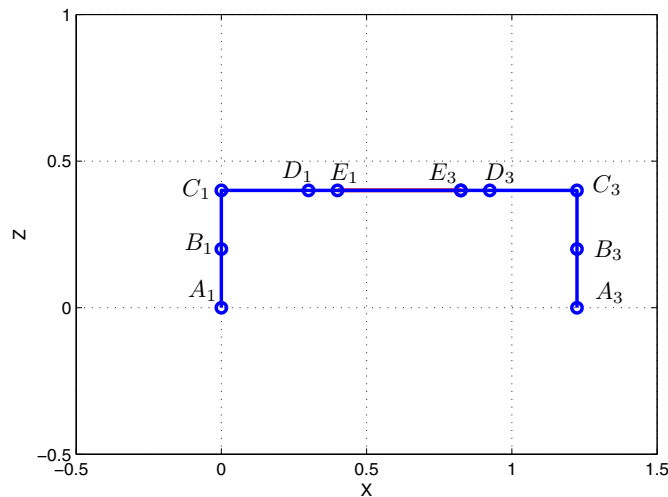


Fig. 6. Side view for the first condition of singularity.

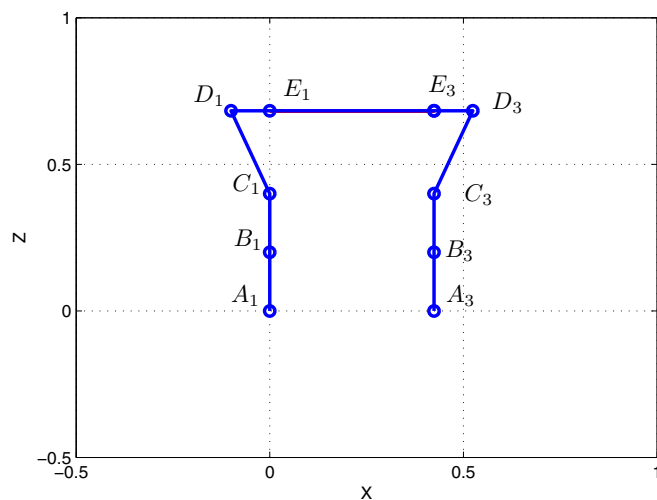


Fig. 7. Side view for the second condition of singularity.

The first condition of singularity, $\theta_{2_l} = 0, \pi, \dots, n\pi$, means that L_2 is fully aligned with L_3 . See Fig. 6.

The second condition of singularity, 52, means that joints E_l, C_l e B_l are vertically aligned in the same plane. See Fig. 7.

Provided that there are three parallel or coplanar axes, a singularity configuration will occur. (Murray et al., 1994)

In such a configuration, we say that the output link loses one or more degrees of freedom; this implies that the output link can resist to one or more components of force or moment with no torque or force applied at the powered joints. This condition can be useful if the robot needs to support heavy loads, forces or torques with little effort or low power consumption.

3.1.2 Direct kinematics singularity of the platform:

This kind of singularity occurs when

$$\det(J_x) = 0. \quad (54)$$

This corresponds to configurations in which the platform is locally movable with all the actuated joints locked. The values of the output variables from given values of the input variables should be obtained. Since, in this case, the nullspace of J_x is non-empty, there exists nonzero output rate vectors \dot{x} which are mapped into the origin by J_x , i.e., which will correspond to null velocities of the input joints.

According to 46, $\det(J_x)$ is null when $\det(J_{x_1}) = 0$ or $\det(J_{x_2}) = 0$.

Matrix J_{x_1} can be square, for example, when the robot is clinging to the surface with two legs, while the other two are in the air. Thus, the matrix J_{x_1} has size 6×6 and singularity occurs when $\det(\Omega_{F_j} - \Omega_{F_k}) = 0$ for $j \neq k$.

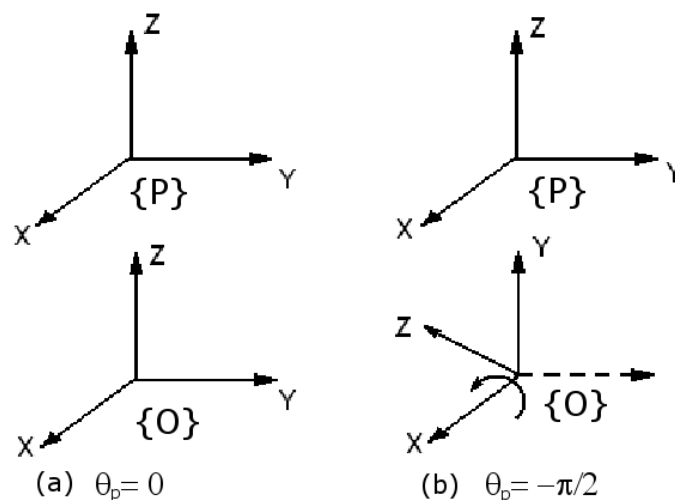


Fig. 8. Singularities for $\theta = 0$ (a) and $\theta = -\frac{\pi}{2}$ (b)

On the other hand, $\det(J_{x_2}) = 0$ for $\theta = 0, \pi, \dots, n\pi, \forall n \in N$. This singularity is associated with the Euler angle convention used. For the Z-Y-Z Euler angle convention, this kind of singularity will occur for all horizontal orientations of the platform. Since this situation is not allowed in this particular application, this problem can be solved by either changing the Euler angle convention or by changing the coordinate system assigned to the climbing surface $\{O\}$ as in Fig. 8, (Harib & Srinivasan, 2003). Now the singularity will occur for $\theta = \frac{\pi}{2}, \frac{3\pi}{2}, \dots, \frac{(2n+1)\pi}{2}, \forall n \in N$, which means that the platform is completely at vertical with respect to the gripping surface (situation rather unlikely to occur in our case).

In such a configuration, we say that the output link gains one or more degrees of freedom, which implies that the output link cannot resist one or more components of force or moment even when all actuators are locked.

3.1.3 Combined singularities of the platform:

The third kind of singularity is of a slightly different nature since it requires conditions on the linkage parameters. This occurs when, for certain configurations, both $\det(J_x)$ and $\det(J_q)$ become simultaneously singular. If some specific conditions on the linkage parameters are satisfied, the chain can reach configurations at which the relation given by 45 degenerates.

This corresponds to configurations at which the chain can undergo finite motions when its actuators are locked or at which a finite motion at the inputs produces no motion at the outputs (Tsai, 1999).

3.2 Jacobian matrix for the leg

The study of the singularity of the leg is similar to the analysis of the serial manipulator attached to point E_l . Differently from the analysis of singularity of the platform, when the rank of the Jacobian of the serial manipulator loses its full rank (singularity condition), it may only lose degrees of freedom.

$$\vec{v}_{A_l} = J_{A_l} \dot{\vec{x}}_{A_l} \quad (55)$$

where:

$$\dot{\vec{x}}_{A_l} = \begin{bmatrix} E_l v_{A_{x_l}} \\ E_l v_{A_{y_l}} \\ E_l v_{A_{z_l}} \\ \dot{\phi}_l \end{bmatrix} \quad (56)$$

To calculate the J_{g_l} is necessary to difference equation 10 relative to time.

$$J_{A_l} = \begin{bmatrix} -s\theta_{1_l}(c\theta_{2_l3_l}\bar{L}_4 + c\theta_{2_l}L_3 + L_2) & (-s\theta_{2_l3_l}\bar{L}_4 - s\theta_{2_l}L_3)c\theta_{1_l} & -s\theta_{2_l3_l}\bar{L}_4 & 0 \\ c\theta_{1_l}(c\theta_{2_l3_l}\bar{L}_4 + c\theta_{2_l}L_3 + L_2) & (-s\theta_{2_l3_l}\bar{L}_4 - s\theta_{2_l}L_3)s\theta_{1_l} & -s\theta_{2_l3_l}\bar{L}_4 & 0 \\ 0 & c\theta_{2_l3_l}\bar{L}_4 - c\theta_{2_l}L_3 & c\theta_{2_l3_l}\bar{L}_4 & 0 \\ 0 & 0 & 0 & 1 \end{bmatrix} \quad (57)$$

In this case, the singularity of matrix J_{g_l} occurs when $\det(J_{g_l}) = 0$. This condition is present for $c\theta_{2_l3_l}\bar{L}_4 + c\theta_{2_l}L_3 + L_2 = 0$ or in other words when:

$$s\theta_{2_l} = \frac{s\theta_{3_l}\bar{L}_4L_2 \pm (c\theta_{3_l}\bar{L}_4 + L_3)\sqrt{\bar{L}_4^2 + 2c\theta_{3_l}L_3\bar{L}_4 + L_3^2 - L_2^2}}{\bar{L}_4^2 + 2c\theta_{3_l}L_3\bar{L}_4 + L_3^2} \quad (58)$$

where:

$$c\theta_{3_l} \geq \frac{L_2^2 - L_3^2 - \bar{L}_4^2}{2L_3\bar{L}_4} \quad (59)$$

Another case of singularity of the leg, but, on the border of the workspace, occurs when a leg is fully extended horizontally as shown in Figure 11. This kind of singularity is due to condition $z_{AE_l} = 0$.

4. Dynamics model

The dynamics of walking machines involves special features that render these systems more elaborate from the dynamics viewpoint, for they present a time-varying topology. What this means is that these systems include kinematic loops that open when a leg takes off and open chains that close when a leg touches the ground (Angeles, 2007). This fact implies in a degree of freedom time-varying. (Pfeiffer et al., 1995).

There are some techniques to analyze the dynamics of robots. In this section, two different methods will be used. Firstly, for the analysis of the dynamics of the platform, the Principle of Virtual Works is used and, for the analysis of the dynamics of the leg, the Newton-Euler formulation is chosen. In both cases, the notations used in (Tsai, 1999) are employed.

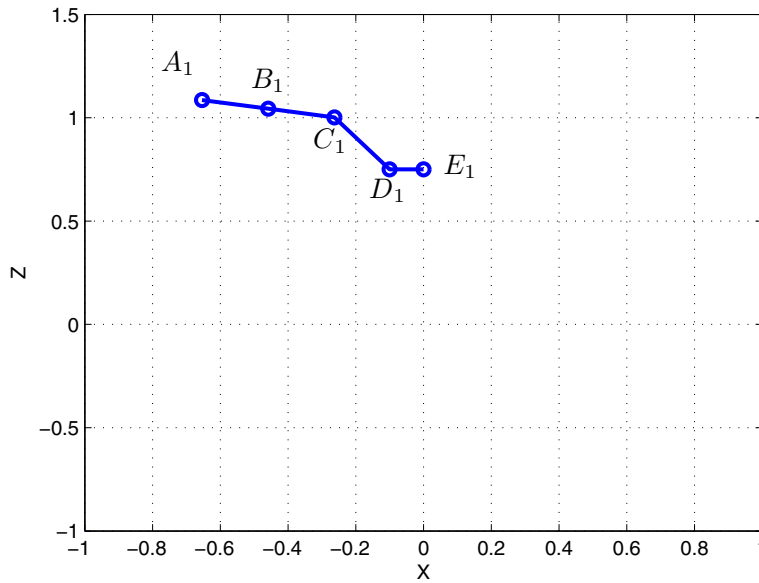


Fig. 9. Singular configuration for the leg in the ar and $\theta_{3_1} = -\frac{\pi}{4}$. First solution.

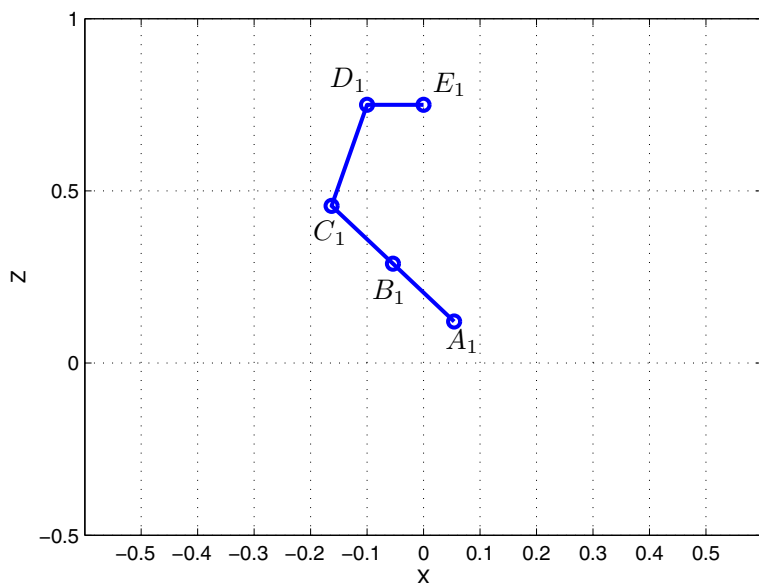


Fig. 10. Singular configuration for the leg in the ar and $\theta_{3_1} = -\frac{\pi}{4}$. Second solution.

- f_{i_l} : resulting force (excluding the actuator force) exerted at the center of mass of link i of leg l .
- $f_{i_l}^*$: inertia force exerted at the center of mass of link i of leg l , $f_{i_l}^* = -m_{i_l} \ddot{v}_{i_l}$
- $\hat{f}_{i_l} = f_{i_l} + f_{i_l}^*$
- f_p : resulting force exerted at the center of mass of the moving platform.
- f_p^* : inertia force exerted at the center of mass of the moving platform, $f_p^* = -m_p \ddot{v}_p$
- $\hat{f}_p = f_p + f_p^*$

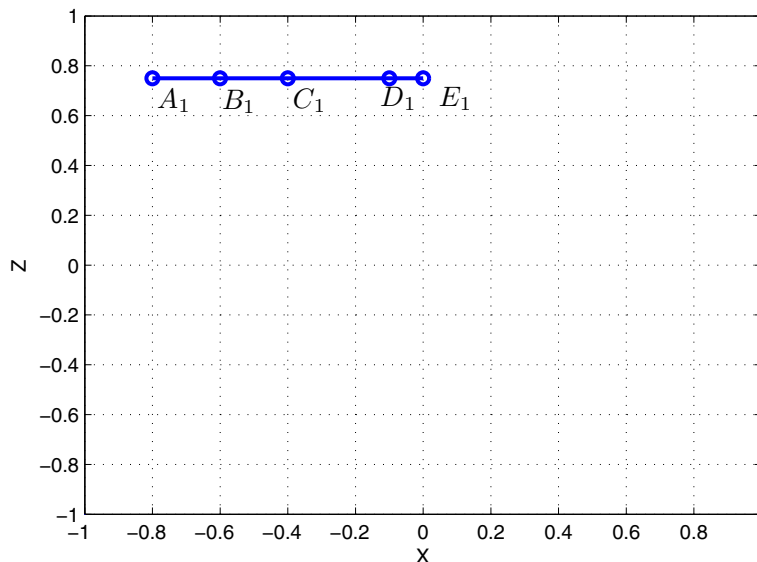


Fig. 11. Singular configuration in the border of the workspace for the leg in the ar.

- n_i : resulting torque (excluding the actuator torque) exerted at the center of mass of link i of leg l .
- n_i^* : inertia torque exerted at the center of mass of link i of leg l , $n_i^* = -{}^i I_i \dot{\vec{\omega}}_i - {}^i \vec{\omega}_i \times ({}^i I_i \vec{\omega}_i)$
- $\hat{n}_i = n_i + n_i^*$
- n_p : resulting torque exerted at the center of mass of the moving platform.
- n_p^* : inertia torque exerted at the center of mass of the moving platform, $n_p^* = -I_p \dot{\vec{\omega}}_p - \vec{\omega}_p \times (I_p \vec{\omega}_p)$
- $\hat{n}_p = n_p + n_p^*$
- x_i : six-dimensional vector describing the position and orientation of link i of leg l .
- $\delta(\cdot)$: virtual displacement of (\cdot) .
- $\vec{\tau} = [\tau_1, \tau_2, \dots, \tau_n]$: vector of actuator torques applied at the active joints $1 \leq i \leq n$ at the leg $l = 1, 2, \dots, 4$

In addition, the next vectors are defined:

$$\hat{F}_i = \begin{bmatrix} \hat{f}_i \\ \hat{n}_i \end{bmatrix}$$

where $i \in A, 1 \leq i \leq 4$, and

$$\hat{F}_p = \begin{bmatrix} \hat{f}_p \\ \hat{n}_p \end{bmatrix}.$$

As the velocities and accelerations of the robot are low, without losing accuracy, it is possible to assume that the link has its mass lumped at its center of mass. This approach was demonstrated in Almeida & Hess-Coelho (2010) sufficiently accuracy for modeling purposes. In both cases, the methods do not take into account all the effects that act on the joints and links. They consider only the dynamics of the rigid body under the action of gravity. A very

important force that was not included in the model is the friction force. As each joint of the Kamambaré is subject to reduction gears, in these circumstances the effects of friction can represent up to 25% of torque needed to trigger a joint in typical situations (Craig, 1989). The effects of viscous and Coulomb friction can then be modeled by a simplified equation:

$$\tilde{\tau}_{i_l} = c \cdot \text{sgn}(\dot{\theta}_{i_l}) + b \cdot \dot{\theta}_{i_l} \quad (60)$$

where b and c are constants.

4.1 Dynamics model of the platform

The Principle of Virtual Work can be written as:

$$\delta q^T \vec{\tau} + \delta \vec{x}_p^T \hat{F}_p + \sum_{l=1}^2 \sum_{i=1}^n \delta \vec{x}_{i_l}^T \hat{F}_{i_l} = 0 \quad (61)$$

As usual, the virtual displacement must be compatible with both the geometrical and kinematical constraints of the system. It is thus necessary to express the displacement as a function of a set of independent generalized virtual displacements. In accordance with that, it is convenient to choose the coordinates of the moving platform \vec{x}_p as the generalized coordinates (Merlet, 2006; Tsai, 1999).

Denoting by J_p and J_{i_l} the jacobian matrices, respectively, of the moving platform and of the link:

$$\delta \vec{x}_{i_l} = J_{i_l} \delta \vec{x}_p \quad (62)$$

and

$$\delta \vec{q} = J_p \delta \vec{x}_p, \quad (63)$$

then equation 61 leads to

$$\vec{\tau} = -J_p^{-T} (\hat{F}_p + \sum_{l=1}^2 \sum_{i=1}^n (J_{i_l}^T \hat{F}_{i_l})). \quad (64)$$

In addition to 64, a more accurate model of the leg dynamics could include various sources of flexibility, deflection of the links under load and vibrations (Bobrow et al., 2004). Nevertheless, this model is sufficiently accurate for our purposes since these effects are not significant for the leg under consideration.

Due to the fact, that the number of actuators is greater than the number of degrees of freedom of the robot, there is an infinite number of solutions for $\vec{\tau}$. Hence, a minimum norm solution can be adopted by applying the pseudo-inverse technique.

To solve equation (64), it is necessary to compute: i) the linear and angular velocities of each link, performing the inverse kinematics analysis; ii) the jacobian matrices of the links and of the moving platform; iii) the forces and torques of the links and of the moving platform.

4.2 Dynamics model of the leg

For the analysis of the dynamics model of the leg, the recursive Newton-Euler formulation was chosen. This formulation uses all the forces acting on the individual links of the robot leg. Hence, the resulting dynamical equation includes all the forces of constraint between two adjacent links.

The method consists of a forward computation of the velocities and accelerations of each link, followed by a backward computation of the forces and moments in each joint. (Tsai, 1999)

4.2.1 Forward computation

The first step is to calculate the angular velocity, angular acceleration, linear velocity and linear acceleration of each link. The best form to calculate these velocities is using a recursive algorithm starting at the first moving link and advancing to the gripper.

$${}^{i+1}\omega_{i+1} = {}^{i+1}R_{i_i} \cdot {}^i\omega_i + \dot{\theta}_{i+1} \cdot {}^{i+1}\hat{Z}_{i+1} \quad (65)$$

where ${}^{i+1}\hat{Z}_{i+1}$ is the versor of the joint axe expressed in the frame $\{i_l + 1\}$ and ${}^{i+1}\omega_{i+1}$ is the angular velocity of joint $i_l + 1$.

$${}^{i+1}\dot{\omega}_{i+1} = {}^{i+1}R_{i_i} \cdot {}^i\dot{\omega}_i + \ddot{\theta}_{i+1} \cdot {}^{i+1}\hat{Z}_{i+1} + {}^{i+1}R_{i_i} \cdot {}^i\omega_i \times \dot{\theta}_{i+1} \cdot {}^{i+1}\hat{Z}_{i+1} \quad (66)$$

$${}^{i+1}v_{i+1} = {}^{i+1}R_{i_i} ({}^i v_i + {}^i\omega_i \times {}^i 0_{i+1}) \quad (67)$$

$${}^{i+1}\dot{v}_{i+1} = {}^{i+1}R_{i_i} [{}^i\dot{\omega}_i \times {}^i 0_{i+1} + {}^i\omega_i \times ({}^i\omega_i \times {}^i 0_{i+1}) + {}^i\dot{v}_i] \quad (68)$$

For the calculation, it is assumed that velocities of base ω_0 , $\dot{\omega}_0$, v_0 and \dot{v}_0 are known and are equal to the platform.

If the center of mass of each link ${}^{i+1}O_{C_{i+1}}$ is known, its acceleration may be calculated by equation 69.

$${}^{i+1}\dot{v}_{c_{i+1}} = {}^{i+1}\dot{\omega}_{i+1} \times {}^{i+1}O_{C_{i+1}} + {}^{i+1}\omega_{i+1} \times ({}^{i+1}\omega_{i+1} \times {}^{i+1}O_{C_{i+1}}) + {}^{i+1}\dot{v}_{i+1} \quad (69)$$

where ${}^{i+1}\dot{v}_{c_{i+1}}$ is the velocity of the center of mass of link $i_l + 1$.

4.2.2 Backward computation

Once the velocities and accelerations of the link are calculated, the joint forces and moments can be computed, one link at time, starting from the gripper and ending at the platform.

$${}^i\hat{f}_i = {}^iR_{i+1} \cdot {}^{i+1}f_{i+1} + {}^i\hat{f}_i^* \quad (70)$$

$${}^i n_i = {}^i n_i^* + {}^iR_{i+1} \cdot {}^{i+1}n_{i+1} + {}^i 0_{c_i} \times {}^{i+1}\hat{f}_{i+1}^* + {}^i 0_{i+1} \times {}^iR_{i+1} \cdot {}^{i+1}f_{i+1} \quad (71)$$

Finally, the torques are obtained by projecting the forces or moments onto their corresponding joint axes.

$$\tau_i = {}^i n_i^T \cdot {}^i\hat{Z}_i \quad (72)$$

5. Illustrative example of the robot gait

This section, presents the performance of the robot in stages I and II (see figure 2). For this, we want to displacement of the center of the platform ${}^O P$ along the Y axis relative to frame $\{O\}$ from the point ${}^O P(0) = [0.392, 0, 0.231]$ to the point ${}^O P(I) = [0.392, 0.39, 0.231]$. At the starting point, legs $l = 1, 3$ are stuck to the surface and legs $l = 2, 4$ are in the air. Frame O is attached to point ${}^O A_1$ like in figure 12.

Table 3 show the control parameters used in this example.

Where N is the fator of discretization of the signals, t_f the time to execute the task, and I_{max_i} and V_{max_i} the maximus values of the current and voltage than can be apply to the joints motors.

In this case some conditions must be respected:

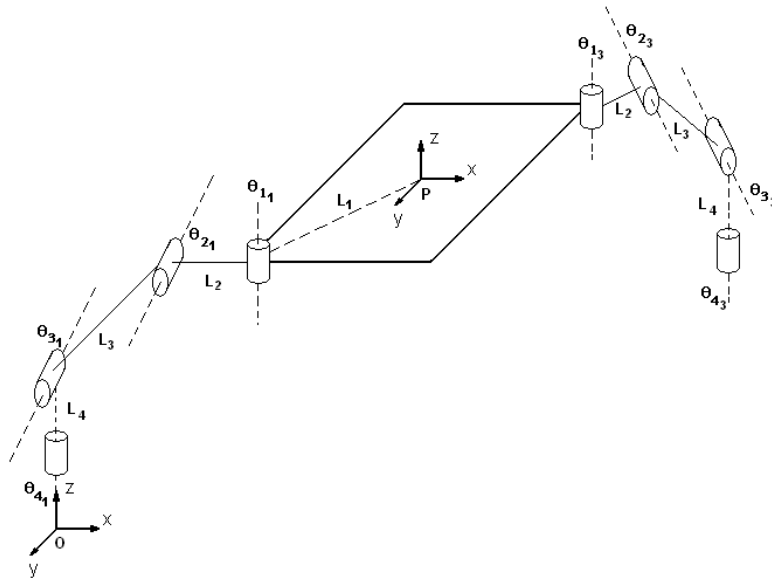


Fig. 12. Mechanical model

Parameters	Movement of the Platform	Movement of the Legs
N	100	100
t_f	40s	60s
$I_{max_{i_j}}$	3.5A	2.8A
$V_{max_{i_j}}$	12v	12v

Table 3. Control Parameters

1. Vector ${}^O A_l \vec{B}_l$ is always orthogonal to the surface in the pushing stage.
2. The legs in the air are locked when the platform is moving.
3. At the pushing stage, joints θ_{1_i} are passives.

The robot move was controlled by an optimal control law that minimize the loss energy in the actuator. The law of control was based in the independent joints control strategy. The objective of the simulation is to show the performance of the system in a basic cycle gait. The gait control was implemented according with the flowchart showed in figure 13.

Figures 14, 15 and 16 show the characteristics of the robot move at the “pushing stage”.

When the desirable position of the platform is reached, the next step is to move the legs that are in the air to the next clinging point. At this moment the stage “leg on the air” begins. Figures 17, 18 and 19 show the performance of one leg in this stage. The orientation of the gripper is the same all the time and it is $\varphi = 0$

When the four legs are clung to the surface, the basic cycle gait is over, and the robot is ready to calculate the new path to go. The total displacement of the robot was from position ${}^O P(0)$ to position ${}^O P(1)$ with an average speed of displacement in the Y axis of about ${}^O \bar{v}_Y = 0.00975m/s$.

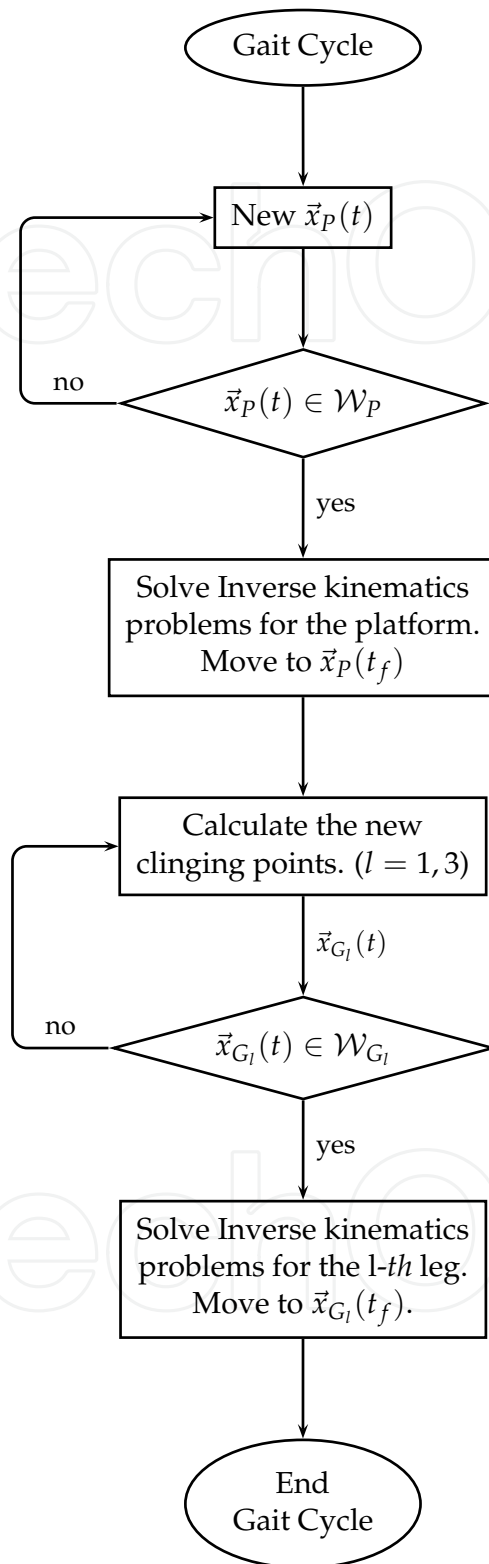


Fig. 13. Control flowchart for a cycle gait

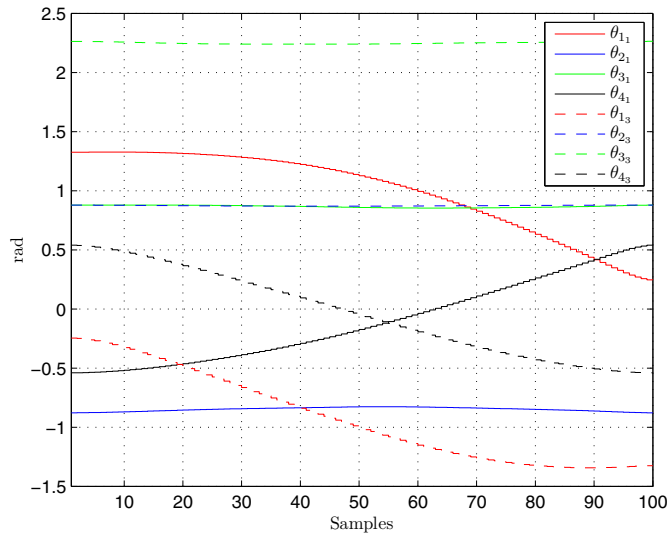


Fig. 14. Joint space in the “pushing stage”.

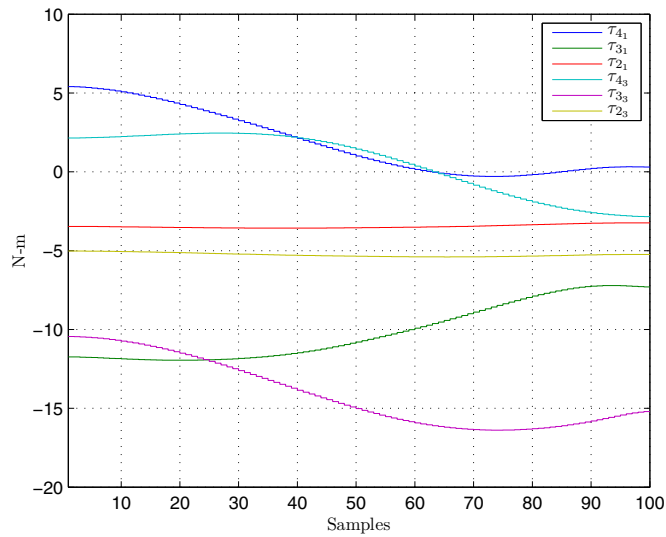


Fig. 15. Joint torques in the “pushing stage”.

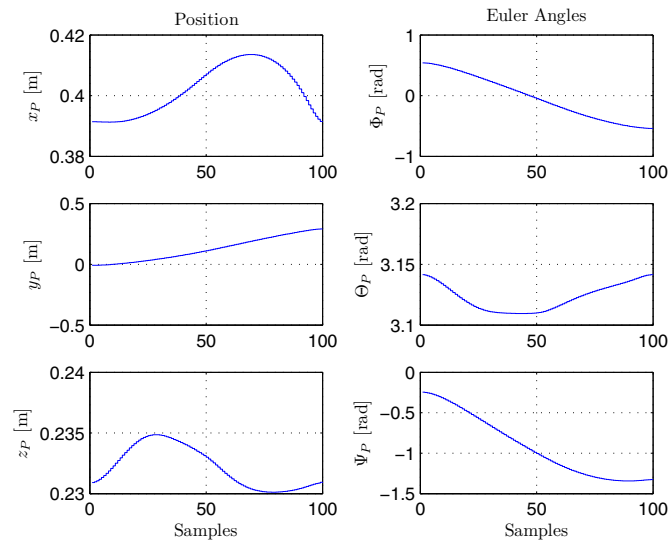


Fig. 16. Movement and orientation of the center of platform in the Cartesian space in the "pushing stage".

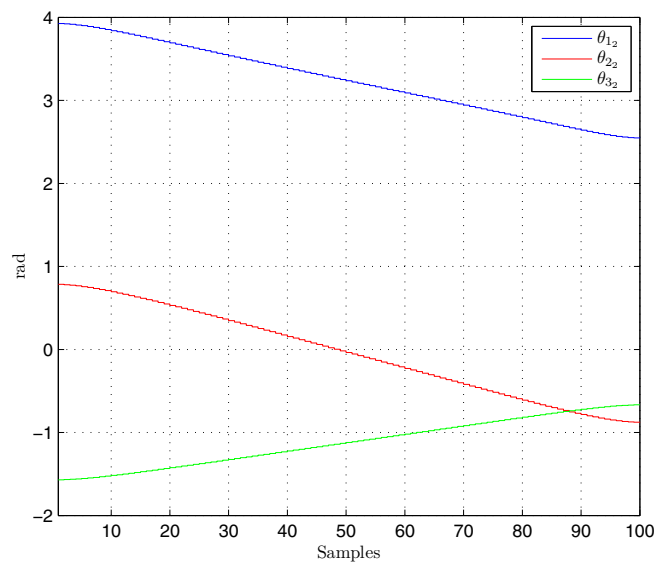


Fig. 17. Joint space for one leg 1 in the stage "leg on the air".

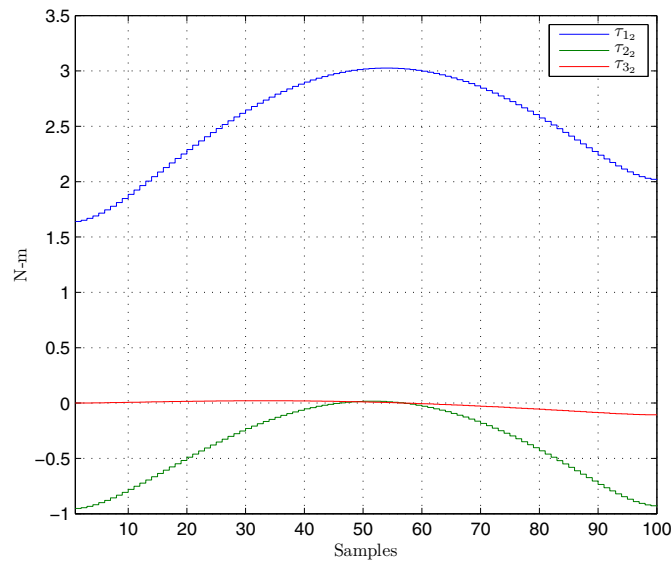


Fig. 18. Joint torques for one leg 1 in the stage “leg on the air”.

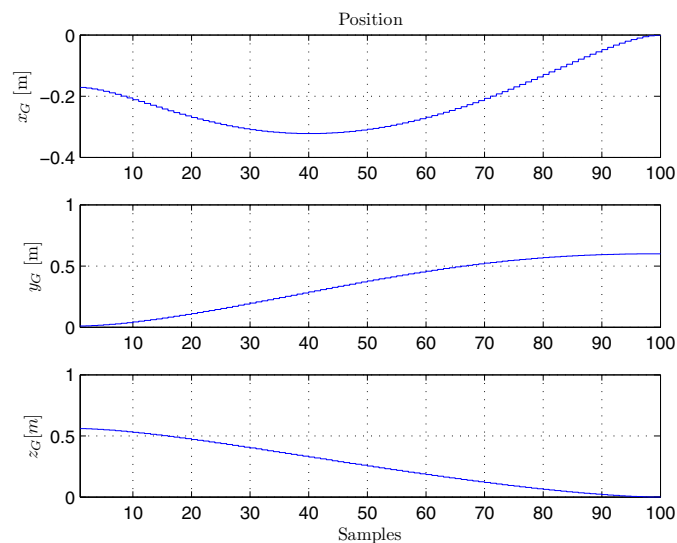


Fig. 19. Movement of the gripper of a leg 1 in the Cartesian space in the stage “leg on the air”.

6. Conclusion

This paper discussed an important issue related to legged robots: the kinematics and dynamics model of the quadruped robot. The analysis done for each model was always presented in two parts, the platform and the legs, according to a time-varying topology and a time-varying degree of freedom of the system.

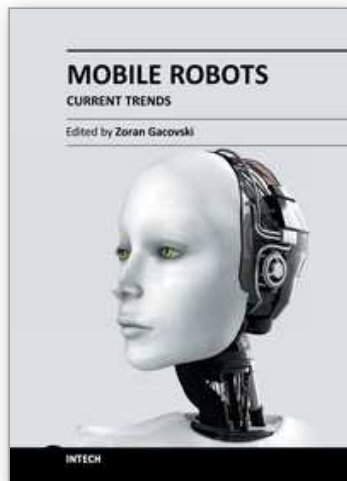
Several methods were used in each modeling process always trying to use those which brought to better performance in accordance with the topology modeled and that could be easily implemented in programming languages of high level. Then were used the Denavit-Hartenberg parameters for solving the direct position kinematics of the platform and leg, the Principle of Virtual Work or the d’Alembert for dynamic modeling of the platform and the Newton-Euler dynamic model for leg in the air.

Special attention was given in the section of the singularities, where the study of all the singularities in the parallel topology were presented. For that, the complete criterion of singularity for parallel robots proposed in Goselin & Angeles (1990) was used. In addition, the principals configurations of the singularities were showed through figures.

Finally, the performance of the robot in a cycle gait was presented. As a result of this example, the space joints, the torque of the joints and the cartesian space relative to this gait were displayed in figures.

7. References

- Almeida, R. Z. H. & Hess-Coelho, T. A. (2010). Dynamic model of a 3-dof asymmetric parallel mechanism, *The Open Mechanical Engineering Journal* 4.
- Angeles, J. (2007). *Fundamentals of Robotic Mechanical Systems. Theory, Methods, and Algorithms*, Springer.
- Bernardi, R. & Da Cruz, J. J. (2007). Kamanbaré: A tree-climbing biomimetic robotic platform for environmental research., *International Conference on Informatics in Control, Automation and Robotics (ICINCO)*.
- Bernardi, R., Potts, A. S. & Cruz, J. (2009). An automatic modelling approach to mobile robots, in F. B. Troch (ed.), *International Conference on Mathematical Modelling, MATHMOD*, Vienna, pp. 1906–1912.
- Bobrow, J., Park, F. & Sideris, A. (2004). Recent advances on the algorithmic optimization of robot motion., *Technical report*, Department of Mechanical and Aerospace Engineering, University of California.
- Craig, J. (1989). *Introduction to Robotics. Mechanics and Control*, Addison Wesley Longman.
- Estremera, J. & Waldron, K. J. (2008). Thrust control, stabilization and energetics of a quadruped running robot, *The International Journal of Robotics Research* 27(10): 1135–1151.
- Goselin, C. & Angeles, J. (1990). Singularity analysis of closed-loop kinematic chains, *IEEE Transactions on Robotics and Automation* 6: 281–290.
- Harib, K. & Srinivasan, K. (2003). Kinematic and dynamic analysis of stewart platform-based machine tool structures, *Robotica* 21: 241–254.
- Kolter, J. Z., Rodgers, M. P. & Ng, A. Y. (2008). A control architecture for quadruped locomotion over rough terrain, *Technical report*, Computer Science Department, Stanford University, Stanford.
- Lenarcic, J. & Roth, B. (eds) (2006). *Advances in Robots Kinematics. Mechanisms and Motion*, Springer.
- Merlet, J. (2006). *Parallel Robots*, 2nd edn, Springer.
- Murray, R. M., Li, Z. & Sastry, S. S. (1994). *A Mathematical Introduction to Robot Manipulation*, CRC Press.
- Pfeiffer, F., Eltze, J. & Weidemann, H.-J. (1995). The tum walking machine, *Intelligent Automation and Soft Computing. An International Journal* 1: 307–323.
- Pieper, D. (1968). The kinematics of manipulators under computer control., *Technical report*, Department of Mechanical Engineering, Stanford University.
- Potts, A. & Da Cruz, J. (2010). Kinematics analysis of a quadruped robot, *IFAC Symposium on Mechatronics Systems*, Boston, Massachusetts.
- Siegwart, R. & Nourbakhsh, I. R. (2004). *Introduction to Autonomous Mobile Robots*, The MIT Press.
- Tsai, L. (1999). *Robot Analysis. The Mechanical of Serial and Paralel Manipulators*, John Wiley & Sons.



Mobile Robots - Current Trends

Edited by Dr. Zoran Gacovski

ISBN 978-953-307-716-1

Hard cover, 402 pages

Publisher InTech

Published online 26, October, 2011

Published in print edition October, 2011

This book consists of 18 chapters divided in four sections: Robots for Educational Purposes, Health-Care and Medical Robots, Hardware - State of the Art, and Localization and Navigation. In the first section, there are four chapters covering autonomous mobile robot Emmy III, KCLBOT - mobile nonholonomic robot, and general overview of educational mobile robots. In the second section, the following themes are covered: walking support robots, control system for wheelchairs, leg-wheel mechanism as a mobile platform, micro mobile robot for abdominal use, and the influence of the robot size in the psychological treatment. In the third section, there are chapters about I2C bus system, vertical displacement service robots, quadruped robots - kinematics and dynamics model and Epi.q (hybrid) robots. Finally, in the last section, the following topics are covered: skid-steered vehicles, robotic exploration (new place recognition), omnidirectional mobile robots, ball-wheel mobile robots, and planetary wheeled mobile robots.

How to reference

In order to correctly reference this scholarly work, feel free to copy and paste the following:

Alain Segundo Potts and José Jaime da Cruz (2011). A Kinematical and Dynamical Analysis of a Quadruped Robot, *Mobile Robots - Current Trends*, Dr. Zoran Gacovski (Ed.), ISBN: 978-953-307-716-1, InTech, Available from: <http://www.intechopen.com/books/mobile-robots-current-trends/a-kinematical-and-dynamical-analysis-of-a-quadruped-robot>

INTECH
open science | open minds

InTech Europe

University Campus STeP Ri
Slavka Krautzeka 83/A
51000 Rijeka, Croatia
Phone: +385 (51) 770 447
Fax: +385 (51) 686 166
www.intechopen.com

InTech China

Unit 405, Office Block, Hotel Equatorial Shanghai
No.65, Yan An Road (West), Shanghai, 200040, China
中国上海市延安西路65号上海国际贵都大饭店办公楼405单元
Phone: +86-21-62489820
Fax: +86-21-62489821

© 2011 The Author(s). Licensee IntechOpen. This is an open access article distributed under the terms of the [Creative Commons Attribution 3.0 License](#), which permits unrestricted use, distribution, and reproduction in any medium, provided the original work is properly cited.

IntechOpen

IntechOpen